Stability of an acid activated carbon based bifunctional catalyst for the raw bio-oil hydrodeoxygenation

Tomás Cordero-Lanzac [a], Roberto Palos [a], José M. Arandes [a], Pedro Castaño [a,*],
José Rodríguez-Mirasol [b], Tomás Cordero [b], Javier Bilbao [a]

[a] Department of Chemical Engineering, University of the Basque Country UPV/EHU, P.O. Box 644-48080, Bilbao, Spain
[b] Universidad de Málaga, Department of Chemical Engineering, Campus de Teatinos s/n 29010, Málaga, Spain

A B S T R A C T

The performance (activity, selectivity and stability) of a Pt-Pd catalyst supported on a phosphorus-containing activated carbon (ACP) has been studied in the hydrodeoxygenation (HDO) of raw bio-oil, and compared with another bifunctional catalyst prepared with a FCC (Fluid Catalytic Cracking) catalyst as acid support. Experiments have been carried out in a fixed bed reactor under the following conditions: 400–450 °C; 65 bar; space time, 0.18 g_{cat} h $g^{-1}_{bio-oil}$; H_2:bio-oil ratio, 20 cm^3$_{H2}$ (STP) cm^{-3}$_{bio-oil}$; time on stream, 0–10 h. The catalyst reaches a pseudo-steady state at 450 °C after 6 h of time on stream, preserving a constant activity as a consequence of the simultaneous formation and hydrocracking of the deposited coke. In these conditions, the yield of C_{5+} hydrocarbons is 20 wt%. This organic liquid fraction mainly contains aromatics, and thus, it may require an additional mild hydrocracking treatment for its valorization as fuel. On the other hand, the gas fraction obtained can be used directly as fuel, and the aqueous liquid fraction (with a high concentration of methanol, 58 wt%) is interesting as co-feedstock with methanol in a methanol to olefins (MTO) unit.

© 2016 Elsevier B.V. All rights reserved.

1. Introduction

Fast pyrolysis of lignocellulosic biomass is an attractive process to obtain fuels and raw materials. An advantage of this route in relation to the other ones from biomass, is that it can be carried out in geographically delocalized units, and its liquid product (bio-oil) can be valorized at large scale in refinery units. Moreover, fast pyrolysis technology has been extensively developed and it allows for obtaining up to 75 wt% of bio-oil in relatively simple units and involving production costs lower than the required ones for competing technologies based on other thermochemical routes [1–3].

Bio-oil contains hundreds of organic compounds mostly in low concentrations (acids, alcohols, aldehydes, esters, ketones, and a large proportion (20–30 wt%) of lignin-derived phenols) [4], with a significant amount of water (up to 50 wt%). Its main properties (poor stability, low heating value, poor volatility, corrosiveness, high viscosity) exclude its direct usage as internal combustion engine fuel. This drawback has encouraged several transformation routes for enhancing its composition [5,6]. Main strategies are: (i)

bio-oil cracking-deoxygenation; associated with pyrolysis, using an acid catalyst (usually a zeolite) in situ in the pyrolysis reactor [7,8], or in a fixed bed reactor coupled on-line in order to transform pyrolysis reactor effluents [9,10]; (ii) bio-oil hydrodeoxygenation (HDO); even though it requires a high H_2 consumption and working at relatively harsh conditions, it allows for obtaining a product with enhanced quality for fuel applications [11,12]. Reactions that take place in the HDO process are [13]: hydrogenolysis of the C–O bond (forming water as a byproduct), dehydration, decarboxylation, hydrogenation of unsaturated compounds and hydrocracking (C–C bond cleavage through a carbocation mechanism).

It is widely assumed that, the large scale bio-oil valorization route requires using the existing refinery infrastructure, co-feeding the bio-oil with the standard feedstock to fluid catalytic cracking (FCC) or to hydroprocessing units [3,14,15]. Considering the versatility of the FCC unit and its presence in most refineries, this route has been extensively studied, particularly using bio-oil model compounds, or its fractions or the pretreated bio-oil (hydrogenated) [16–19]. The results obtained from the cracking of vacuum gas oil (VGO) and raw bio-oil mixture (20 wt%) under FCC conditions, have shown the advantages of co-feeding bio-oil due to the existence of mechanistical synergies between oxygenates and hydrocarbons [20]. On the other hand, this route offers the following disadvan-

tages: low gasoline selectivity and low carbon utilization due to the fact that part of it is converted into CO and CO_2 by decarbonylation and decarboxylation, respectively. Furthermore, feeding a high proportion of bio-oil into the FCC leads to gasoline with high concentration of oxygenates that require further treatments [20].

The hydroprocessing of bio-oil and its oxygen containing model compounds is interesting because it is less limited than their cracking, and can be tuned in order to obtain a fuel directly or to partially deoxygenate bio-oil [21,22], with the disadvantage of using hydrogen in the unit. Hydroprocessed bio-oil has been used in turbines [23,24] or for a subsequent valorization through cracking or hydrocracking (targeting the conversion of phenols and furans) [25]. The range of operating conditions studied for hydroprocessing bio-oil, in terms of pressure and temperature, is very wide [14], as well as the catalysts studied: noble metals (Pt, Pd, Ru, Rh) and transition metals (Ni, Mo, Co, W) based catalysts, bimetallic catalysts (Pt-Pd, Rh-Pd, Pt-Sn, NiMo, NiW, NiCo, CoMo), among many others. The catalyst supports studied include Al_2O_3, γ-Al_2O_3, ZrO_2, TiO_2, MgO, mesoporous zeolites and activated carbons [26]. The acidic sites in the bifunctional catalysts are of vital importance to deoxygenate the most refractory compounds of bio-oil, specially phenols, owing to the simultaneous methyl transfer and hydrodeoxygenation reactions [27,28].

The activated carbons (ACs) have shown promising performance in this HDO of bio-oil due to their chemical stability, high specific surface area, tailored pore size distribution for specific reactions and their capacity to be functionalized and prepared with different physical shapes (granules, extrudates, pellets, fibers, etc.) [29]. In addition, they are obtained from different low-cost sources, such as, biomass and wastes and, because of their characteristics, noble and transition metals supported on activated carbons have been used in bio-oil HDO [3,30]. Sanna et al. [31] have studied bio-oil aqueous fraction HDO in two sequenced stages at 125 and 250 °C, with Ru/AC and Pt/AC catalysts, respectively.

The aim of this work is to validate the potential catalytic performance of a Pt-Pd phosphorous-containing activated carbon for a first HDO stage of raw bio-oil process at high temperature (400–450 °C). Our motivation is driven by (i) the outstanding performance of this catalyst for tire-oil hydrocracking [32], and (ii) the requirement of delivering a stable catalyst for bio-oil HDO, which is a process strongly controlled by a severe coke deposition [31]. Two types of bifunctional catalysts (Pt-Pd on phosphorous-containing activated carbon and on FCC catalyst) have been synthesized, characterized and tested in the bio-oil HDO. Coke deposition have been also studied.

2. Experimental

2.1. Catalysts preparation and characterization

Two bifunctional catalysts were prepared, using Pt-Pd as the metallic function and different supports which provide the acidic function: (i) a phosphorous-containing activated carbon (ACP), and; (ii) a commercial equilibrated FCC catalyst (used in an industrial unit, that guarantees the stability of the catalyst). These catalysts were named as Pt-Pd/ACP and Pt-Pd/FCC, respectively.

ACP support was prepared by chemical activation with H_3PO_4 [33]. The lignocellulosic precursor (olive stone) was impregnated with an aqueous solution of H_3PO_4 (85 wt%, 3 g of H_3PO_4 per g of precursor), and then, it was activated in a tubular furnace under a continuous flow of N_2 (150 cm^3 min^{-1}), rising the temperature at 10 °C min^{-1}, up to 500 °C for 2 h. The activated carbon obtained was cooled in the tubular furnace, washed with distilled water at 60 °C (until phosphate was not detected in the eluent), and dried in a vacuum drier at 100 °C. ACP was sieved to a particle size of

100–300 μm. It should be noted that activated carbons prepared by this method show acidic sites which are active in alcohols dehydrations [33–35]. The Pt-Pd/ACP bifunctional catalyst was prepared incorporating Pt and Pd by simultaneous incipient wetting impregnation, with an aqueous solution of $HPtCl_6 \cdot 6HCl$ and $PdCl_2$ slightly acidified with HCl, with the adequate concentration to obtain a nominal value of Pt and Pd of 1 wt% and of 0.5 wt%, respectively. This relation is the adequate one to ensure a high activity and stability of Pt-Pd catalysts in the hydrogenation of phenols [36]. The impregnated support was heat-treated in a tubular furnace with a N_2 flow of 150 cm^3 min^{-1} at 400 °C for 4 h.

On the other hand, the FCC industrial support was tableted and sieved to the same particle size (100–300 μm) and the Pt-Pd/FCC catalyst was prepared by impregnation method at pH = 7 using $Pt(NH_3)_4(NO_3)_2$ and $Pd(NH_3)_4(NO_3)_2$ solutions as metal precursors, followed by water removal at 80 °C in vacuum [37]. The bifunctional catalyst was dried at 100 °C and calcined at 500 °C for 3 h in air. The metallic content of the FCC catalyst was determined by means of inductively coupled plasma-optical emission spectroscopy (ICP-OES) on a Thermo spectrometer (XSeries 2 model), subsequent to subjecting the sample to acid digestion in HF at 90 °C.

Porous structure of the catalysts was characterized by N_2 adsorption-desorption at −196 °C in a Micromeritics ASAP 2020. Samples were previously outgassed for 8 h at 150 °C under vacuum. From N_2 adsorption-desorption isotherm, specific surface was calculated using the BET equation, and micropore volume was calculated using the t-method. Pore size distribution and average pore diameter were also estimated from N_2 adsorption isotherm by BJH method.

TEM analyses were performed on a Philips CM200 microscope equipped with a supertwin lens to study the catalyst morphology; in addition, particle size was calculated by counting particles in different TEM micrographs. The surface chemical state and elemental identity were measured by X-ray photoelectron spectroscopy (XPS) in a 5700C model Physical Electronics apparatus with MgKα radiation (1253.6 eV). The C 1s peak was located at 284.5 eV [38] and it was used as reference to locate the other peaks. Fitting of XPS peaks was done by least squares using Gaussian-Lorentzian peak shapes. Metallic surface and dispersion were determined by CO chemisorption, carried out in a Micromeritics ASAP 2010.

Acidic properties of the catalysts were determined by temperature programmed desorption (TPD) up to 550 °C, of NH_3 previously adsorbed at 150 °C, using a Setaram DSC thermogravimetric-calorimeter analyzer coupled on-line to a Balzers Quadstar 422 mass spectrometer. Samples were firstly submitted to stripping with He at 550 °C. Brønsted and Lewis acidic sites ratio was determined after pyridine adsorption at 150 °C, based on the 1545 and 1455 cm^{-1} FTIR signals ratio, using a Nicolet 6700 apparatus equipped with a Specac catalytic chamber. For these experiments, a tablet of ca. 30 mg of fresh catalyst was prepared by grinding and pressing the grains at 10 t cm^{-2} for 10 min. The tablet was submitted to a heat pretreatment at 380 °C and vacuum, and the signal was recorder with a frequency of 0.2 min^{-1}.

2.2. Bio-oil

Bio-oil was obtained by fast pyrolysis of black poplar sawdust at 440–450 °C, using a pilot plant provided with a conical spouted bed reactor with a capacity of 25 kg h^{-1} [39]. It was characterized (Table 1) by elemental analysis (Leco TruSpec CHN Macro and additional module TruSpec S) to determine the contents of C, H, N, S and O content by difference (it is worth mentioning the negligible N and S contents in the feed), and the concentrations of the component families were determined by GC–MS (Shimadzu GC–MS QP2010, column BPX5; length, 50 m; internal diameter, 0.22 mm). Water

Table 1
Bio-oil composition.

Elemental composition (wt%)	
C	52.2
H	7.1
O	40.7
Water content (wt%)	**49.0**
Composition (wt%)	
Acids and esters	9.5
Acetic acid	23.5
Aldehydes	4.8
Ketones	8.7
1-Hydroxy-2-propanone	7.0
Phenols	13.0
Alcohols	6.5
Ethers	2.0
Levoglucosan	24.0
Non identified	1.0

Table 2
Physico-chemical properties of the catalysts.

	Pt-Pd/ACP	Pt-Pd/FCC
Porous structure		
S_{BET} ($m^2 g^{-1}$)	1305	53
$V_{micropore}$ ($cm^3 g^{-1}$)	0.52	0.01
V_{pore} ($cm^3 g^{-1}$)	1.34	0.13
Metal properties		
$S_{metal.}$ ($m^2 g^{-1}$)	0.91	0.53
Dispersion (%)	19.2	15.3
Acid properties		
Total acidity ($mmol_{NH3} g^{-1}$)	140	15
Brønsted acidic sites (%)	>95	53

content was measured by Karl-Fisher titration method (Metrohm 830 KF Titrino plus).

2.3. Reaction equipment and procedures

The runs were carried out in a laboratory scaled fixed bed reactor described in previous works [40] operating in trickle bed regime, under the following experimental conditions: 400, 425 and 450 °C; 65 bar; space time, 0.18 g_{cat} h $g^{-1}_{bio-oil}$; H_2:bio-oil ratio, 20 cm^3_{H2} (STP) $cm^{-3}_{bio-oil}$; time on stream, 0–10 h. The catalyst diluted in SiC was loaded in the reactor following the procedure described by van Herk et al. [41] in order to minimize the segregation in the loading of the reactor and to obtain an homogeneous bed. Prior to the reaction, the catalysts were reduced in situ at 400 °C for 4 h under a continuous flow of 30 $cm^3 min^{-1}$ of H_2 and 50 $cm^3 min^{-1}$ of N_2. The reaction products were sent to a gas/liquid separator and the gases were analyzed on-line in a Varian CP-4900 microGC provided with four channels: (i) a molecular sieve to separate the permanent gases H_2, O_2, N_2, methane and CO; (ii) a Porapak Q to separate C_2 hydrocarbons and CO_2; (iii) Al_2O_3 to separate C_3 and C_4 hydrocarbons; and (iv) CPSiL to separate C_5–C_{10} hydrocarbons.

Liquids were collected and separated in an aqueous fraction, which was analyzed in the GC–MS aforementioned; and in an organic fraction, analyzed in a two dimensional gas chromatograph (GC × GC), provided with a FID detector and coupled on-line with a mass spectrometer (MS). The equipment used consisted of two columns of different polarity connected by a flow modulator, being the first column a non-polar DB-5MS (length, 30 m; internal diameter, 0.25 mm), while the second one was a polar TRB-50 HT (length, 5 m; internal diameter, 0.25 mm).

Both, aqueous and organic fractions, as well as raw bio-oil, were also characterized through FTIR spectroscopy using the Nicolet 6700 apparatus equipped with a transmission chamber. A drop of the liquid was sandwiched between two tablets of 100 mg of KBr, and was introduced into the transmission chamber. Spectra were recorded with a frequency of 4 cm^{-1}. Liquid products were also analyzed by ^{1}H NMR spectroscopy. Experiments were carried out in a Bruker AV500 spectroscope, equipped with a 5 mm broad band probe. Suppression of residual water signal was necessary in the cases of raw bio-oil and aqueous liquid fraction products due to their high water content, these samples were solved in deuterated water. On the other hand, organic liquid fraction samples were directly solved in deuterated chloroform. The ^{1}H NMR spectra were acquired at 400 MHz and processed with the TOPSPIN 1.3 (Bruker) software.

The solid product deposited on the catalyst was analyzed by temperature programmed oxidation (TPO), performed in a thermobalance (TA Instruments TGA Q5000 IR). In the cases of activated carbon-based catalyst, the carbonaceous support is also burned. Samples were previously submitted to a stripping treatment with N_2 (100 $cm^3 min^{-1}$) at the reaction temperature in order to remove the non-deactivating physically adsorbed species on the catalysts support. TPO analyses were carried out under a continuous 100 $cm^3 min^{-1}$ flow of air using a ramp temperature of 10 °C min^{-1}, up to 900 °C for the ACP-based catalyst and up to 550 °C for the FCC-based catalyst, assuring the complete combustion of the carbonaceous solid in both cases.

### 3. Results and discussion

3.1. Properties of the catalysts

The main physicochemical properties of Pt-Pd/ACP and Pt-Pd/FCC catalysts are displayed in Table 2. Porous textural parameters, obtained from N_2 adsorption-desorption isotherms (Fig. 1a), are significantly different due to the nature of each support. This difference between the catalysts is exposed comparing their isotherms. Both catalysts show a type IV isotherm, and it can be observed how the gas is adsorbed along the whole range of relative pressures. Pt-Pd/ACP catalyst shows a great N_2 adsorption at relative pressures below 0.4 corresponding to micro and mesopores, whereas the Pt-Pd/FCC catalyst adsorbs its biggest amount of N_2 at high relative pressures, (corresponding to the adsorption on macropores). As a consequence of the high-developed activated carbon microporosity, the Pt-Pd/ACP catalyst shows a specific surface of 1305 $m^2 g^{-1}$, with high pore and micropore volumes (1.34 and 0.52 $cm^3 g^{-1}$, respectively). On the contrary, FCC catalyst particles have a hierarchical porous structure as a consequence of the microporous crystals of USY zeolite embedded in a meso and macroporous matrix (accessible to huge molecules fed to the FCC unit) [42]. It explains the lower textural parameters, with a specific surface area of 53 $m^2 g^{-1}$ and values of pore and micropore volumes one order of magnitude lower (0.13 and 0.01 $cm^3 g^{-1}$, respectively). These structural differences between both catalysts can be observed in pore size distribution (Fig. 1b), quantifying the contribution of each pore size fraction to the specific amount of N_2 adsorbed. As it can be appreciated, Pt-Pd/ACP catalyst shows a maximum in 10 Å and a considerable presence of pores under 30 Å, with narrow mesopores ($\approx$ 20 Å) characteristic of activated carbons.

The maximum of the micropore size distribution of the ACP is slightly displaced regarding to the usual one in activated carbons, due to a pore widening phenomenon which takes place in the activation with H_3PO_4 [43]. On the other hand, Pt-Pd/FCC catalyst shows a different pore size distribution, in which a smaller micropore is observed (characteristic of USY zeolite) and a main presence of mesopores of a size bigger than 50 Å, characteristic of the matrix
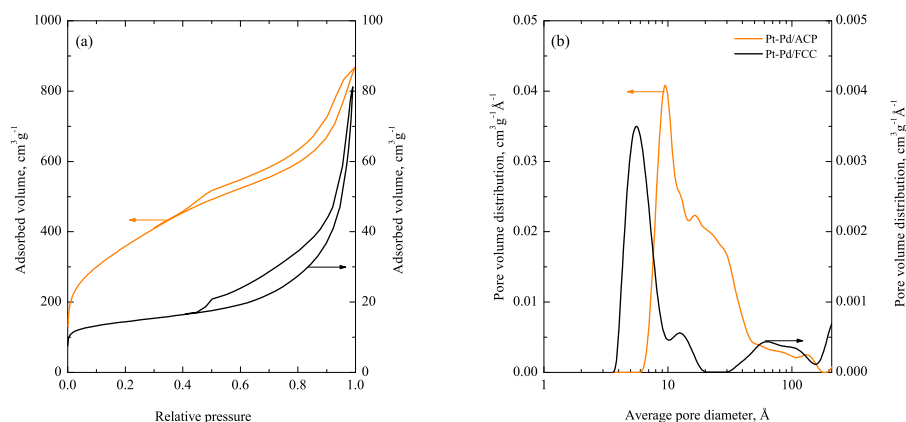
Fig. 1. (a) N$_2$ adsorption-desorption isotherms and (b) pore size distribution for Pt-Pd/ACP and Pt-Pd/FCC catalysts.
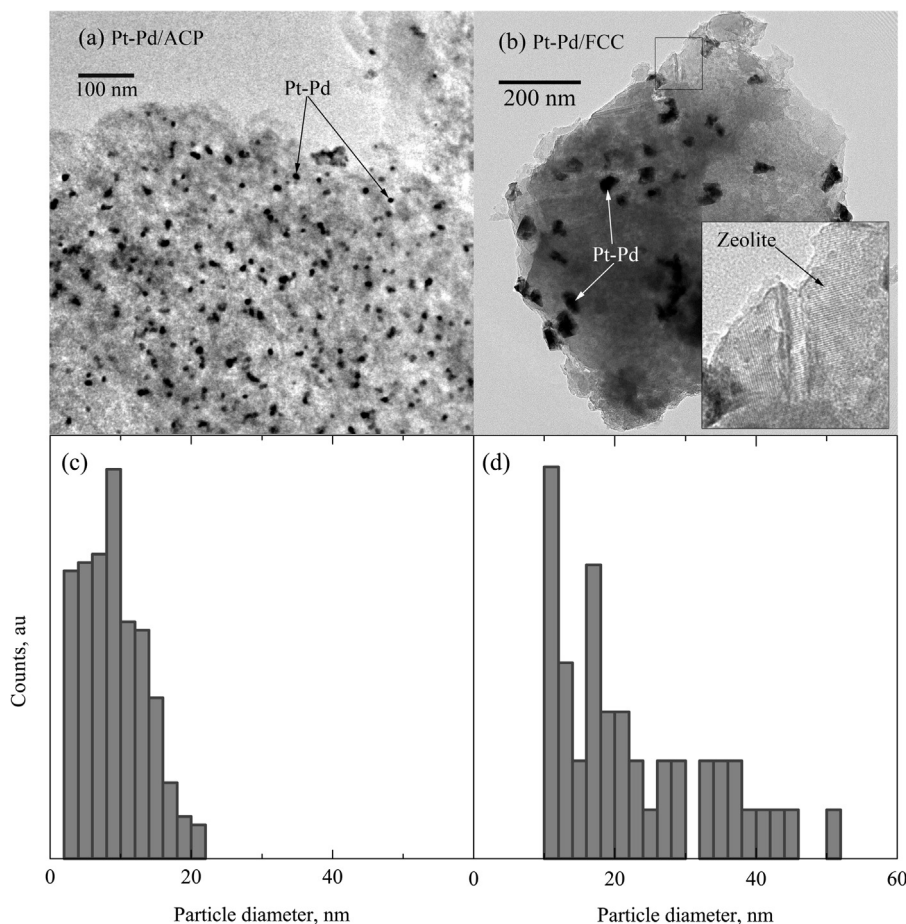
Fig. 2. TEM micrographs for (a) Pt-Pd/ACP and (b) Pt-Pd/FCC catalysts. Pt-Pd particle size distributions histograms for (c) Pt-Pd/ACP and (d) Pt-Pd/FCC catalysts.

of the FCC catalyst. It can be also appreciated the presence of the matrix macropores at wider size (>100 Å).

The properties of the metallic function, shown in Table 2, are quite similar for both catalysts. As observed, the metallic surface, as well as the dispersion, is slightly higher for the Pt-Pd/ACP catalyst (0.91 m^2 g^{-1} and 19.2%, respectively). These results highlight the capability to support Pt and Pd on both supports of different nature (organic and inorganic) and porous structure. XPS analyses reveal that the surface amount of metal is similar to the nominal concentration, which demonstrate that the methods used for loading the metal are efficient and allow for obtaining a uniform dispersion of the metallic function [32]. Fig. 2 shows TEM images

for the catalysts. The well-dispersed nanoparticles of Pt and Pd in the ACP and FCC supports are observed in Fig. 2a and b respectively, however, they do not show a defined geometric form. ACP support shows an amorphous structure, in which Pt and Pd crystals are loaded, typical of activated carbon (Fig. 2a). On the other hand, in the zoomed detail of Fig. 2b, several crystalline planes of the HY zeolite are observed, showing the significant difference in the nature of both catalysts. Fig. 2c and d shows the Pt-Pd particle size distribution for Pt-Pd/ACP and Pt-Pd/FCC catalysts, respectively. As can be observed, Pt-Pd/ACP catalyst exhibits a narrow Pt-Pd particle size distribution centered in 10 nm, whereas, for the Pt-Pd/FCC catalyst, a broader distribution has been obtained, with an important con-
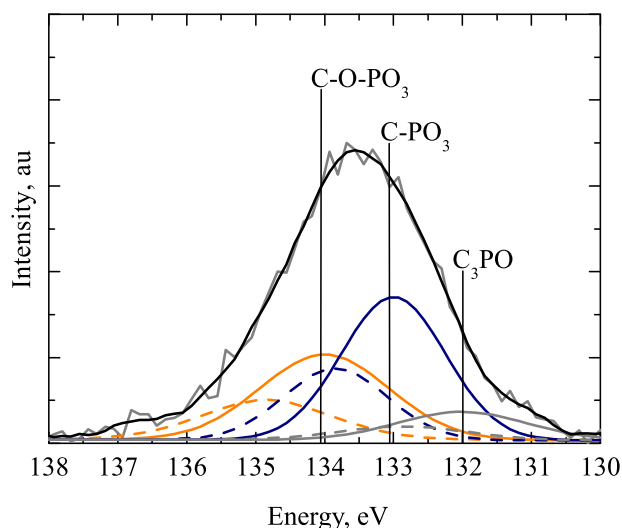
Fig. 3. P 2p spectrum for Pt-Pd/ACP obtained by XPS.

Table 3
Main P groups identified in the activated carbon surface.

Energy (eV)	Functional group	Structure
132	$-C_3PO$	
133.1	$-C-PO_3$	
134.1	$-C-O-PO_3$	

tribution of particles with an average size of 40 nm. These results can be correlated with the apparent Pt-Pd particle sizes showed in TEM micrographs (Fig. 2a and b, please note the different scales of the images).

The acidic features are different among the catalysts used (Table 2). The total acidity of the Pt-Pd/ACP catalyst is 140 $mmol_{NH3}\,g^{-1}$, which is much higher than that registered for the Pt-Pd/FCC catalyst (15 $mmol_{NH3}\,g^{-1}$). Moreover, chemically activated carbons with H_3PO_4 (by this method) exhibit higher proportion of Brønsted type acidic sites (>95% [38] and 53% for the Pt-Pd/FCC catalyst). These results demonstrate the high density of acidic sites provided by the P-groups fixed on the carbon surface and their markedly acidic strength. On the other hand, the poor acidic properties of the equilibrated FCC support are explained by the severe dealumination and dehydroxilation processes at which this support is submitted during the reaction-regeneration cycles in the industrial unit.

Fig. 3 shows the P 2p spectrum of the Pt-Pd/ACP catalyst obtained by XPS analysis, in which is possible to observe the different P-groups of the activated carbon. The spectrum have been deconvoluted in doublet peaks with an area ratio of 0.5 and a peak separation of 0.84 eV [38]. Three main species of phosphorus can be identified which are, from the most reduced to the most oxidized: (i) C_3PO, with the main peak of the doublet located at 132 eV, (ii) C-PO_3 at 133.1 eV and (iii) C-O-PO_3 at 134.1 eV.

The most reduced phosphorous group shows three simple bonds with C atoms of the support and a double bond with the O, and as can be observed in its detailed structure (Table 3) it does not have acidic character. However, the majority of the phosphorus surface groups exhibit structures with the -PO_3 form, which are only bounded to C atoms of the support with a unique simple bond (direct or through an O bond which increases in 1 eV the binding energy). These -PO_3 groups have a double bond with the O and two more simple bonds with -OH groups. As shown in Fig. 3, these kinds of groups are the most abundant ones in the carbon surface and they provide the support with Brønsted acidic sites (because of the protons of the hydroxyl groups) as pyridine analysis has revealed (Table 2).

3.2. Products yield and catalysts stability

Bio-oil hydrodeoxygenation products have been distributed in gas, liquid and solid fractions, being the solid one the coke deposited on the catalysts. The liquid fraction is separated through decanta-tion in two different phases; a less dense organic phase (named organic liquid fraction) and a more dense and abundant aqueous phase (named aqueous liquid fraction). Table 4 summarizes the yields of the gas, liquid organic, liquid aqueous, and solid fractions, corresponding to 6 h of time-on-stream (TOS) for the operating conditions tested. Gas and liquid fractions yields are calculated using the following equation.

$$(Yield)_i = \frac{F_i}{F_{bio\text{-}oil}} 100 \qquad (1)$$

where F_i and $F_{bio\text{-}oil}$ are the mass flow rates corresponding to the i product fractions and the oxygenates in the bio-oil, respectively. Coke yield is an average value obtained from the deposited coke amounts and from the bio-oil fed along the 6 h. It is noteworthy that coke content on the catalyst has been considered to increase linearly with the time-on-stream in order to calculate the mass balance in the product streams. On the other hand, gas yields (shown in Table 4) were compulsory determined by difference using the C mass balance for the bio-oil and products.

The liquid product obtained with the Pt-Pd/ACP catalyst at 400 °C has a unique phase. This may be a consequence of the short advance of dehydration reactions at low temperature and, therefore, the water content in the solution is lower than that necessary for phase separation. A decrease in the aqueous liquid fraction yield is observed upon increasing the temperature from 425 to 450 °C due to the transformation of oxygenates into hydrocarbons, which are insoluble in water. Consequently, organic liquid and gas fraction yields increase.

The solid fraction (coke) is produced by the repolymerization of bio-oil phenols and the yield observed for this fraction is relatively high (29.5 wt% at 400 °C) [44]. This thermal pyrolytic lignin basically deposits on the external surface of the catalyst particles (external coke). Gayubo et al. [45] and Valle et al. [46] have established that using HZSM-5 zeolite as catalyst in bio-oil dehydration/cracking processes, a mechanism of coke formation within the micropores of the zeolite takes place simultaneously to the thermal pyrolytic lignin deposition on the external surface of the catalyst particle. This internal coke generated by condensation of hydrocarbon products in the reaction media and by the evolution of the other coke fractions is the major contributor to catalyst deactivation because it partially blocks the acidic sites of the zeolite. A rise in reaction temperature implies a light reduction in coke yield (until 25.9 wt% at 450 °C) which could be attributed to a boost in the hydrocracking of coke precursor oligomers deposited within the pores. In

Table 4
Product fractions yields for different reaction temperatures. Time on stream, 6 h.

Catalyst	Temperature (°C)	Organic liquid fraction (wt%)	Aqueous liquid fraction (wt%)	Gas (wt%)	Coke (wt%)
Pt-Pd/ACP	400	–	37.2[a]	33.3	29.5
	425	17.2	15.4	40.9	26.6
	450	20.5	10.4	43.2	25.9
Pt-Pd/FCC	450	13.9	27.4	28.9	29.8

[a] No phase separation observed.
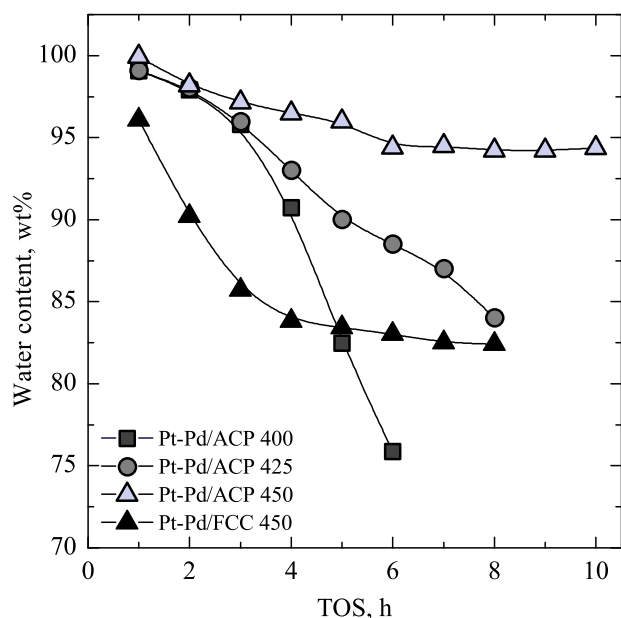
Fig. 4. Evolution with the time on stream of the water content in the aqueous liquid fraction for the Pt-Pd/ACP at three different temperatures and for the Pt-Pd/FCC at 450 °C.

reactions evolving bifunctional catalysts, temperature plays a key role in coke formation and in its elimination via hydrogenation, upon the metallic function; and via cracking, upon the acidic function; and, thus, in deactivation attenuation [47]. An increase in the reaction temperature promotes oligomerization reactions of bio-oil phenols. However, hydrogenation and cracking reaction rates of coke precursors are as well increased [48–50].

Catalyst deactivation is mainly due to the severe coke deposition on the catalyst. Fig. 4 shows the evolution of water content in the aqueous liquid fraction with the TOS. This evolution can be associated to an estimation of the evolution of the apparent activity of the catalyst. In fact, water is the final product of the dehydration reaction of the oxygenates of the bio-oil and of the intermediates of the HDO reaction. A simplified reaction of the HDO of bio-oil can be expressed as:

$$R=O + 2H_2 \rightarrow H\text{-}R\text{-}H + H_2O \qquad (2)$$

As observed in Fig. 4, water content in aqueous liquid fraction decreases as TOS increases. However this decay is attenuated at higher temperatures. Pt-Pd/ACP catalyst reaches a pseudo-steady state at 450 °C with a constant activity after 6 h of TOS. Under these conditions, the catalyst activity is steady due to the fact that coke is being formed at the same rate at which it is being hydrogenated and eliminated. As the catalyst maintains a significant steady activity at this temperature, dehydration rate is still fast and a liquid fraction with 95 wt% of water content is obtained. Fig. 4 shows that Pt-Pd/FCC catalyst also reaches a pseudo-steady state after 4 h of TOS at 450 °C. Nevertheless, this steady activity is notably lower than that registered for Pt-Pd/ACP catalyst (water content of 82 and 95 wt% respectively) as a consequence of the more pronounced

deactivation suffered by the Pt-Pd/FCC catalyst in the initial hours of the reaction.

An important synergy of the hydrogenation, cracking and hydrogen transfer reactions has demonstrated to minimize coke formation and deposition [51]. Gutiérrez et al. [52], have emphasized the role of support acidity in the attenuation of coke formation in the hydrocracking of LCO (light cycle oil, byproduct of the FCC unit) which has a high tendency to form coke due to its high aromatic content (up to 75 wt%).

Pt-Pd/ACP catalyst keeps (Fig. 4) a notable high activity at 450 °C. Besides, a low deactivation rate can be also correlated with a high water content in the reaction media, because this molecule tends to minimize the effect of coke due to the sweeping of the oligomers and internal coke precursors. Several works have demonstrated the hydrothermal stability of the acidic sites of ACP during dehydration of alcohols, where the water content in the reaction media is very high [34,38], and it also shows good stability at this high temperature as support in the hydrocracking of a heavy and aromatic feeding as tire pyrolysis oil [32]. The acidic sites stability attenuates the coke formation. This, along with the characteristic microporous structure and its numberless connections between the pores, ease the coke precursor sweeping and are responsible for the limited coke formation and for the reach of the high steady activity.

The acidic sites of the Pt-Pd/FCC catalyst support have suffered a severe equilibrating treatment with steam and lots of cycles of cracking-regeneration in the FCC unit. Thus, its acidic sites are very stable in the reaction conditions of bio-oil HDO. Additionally, the matrix structure of the FCC catalyst, which allows the diffusion of heavy molecules like asphalthenes in FCC reaction, also favors the sweeping of heavy oligomers and coke precursors in the current reaction conditions. Therefore, both metallic and acidic functions of the catalysts explain the pseudo-steady state at 450 °C. Indeed, the supports are active for converting bio-oil towards products that have less economic interest. But above all, the role of the metallic function of the catalyst is helping reach the pseudo-steady state by providing hydrogen to the coke precursors. In fact, the process becomes unstable when using the bare supports (without the metallic function) because there is a complete blockage of the reactor within the first hours on stream, not having the chance to obtain a representative gas or liquid sample.

Fig. 5 displays the apparent yield of oxygenates (OX, reaction products and non-transformed components of bio-oil) and the yields of the gas and liquid fractions at TOS = 6 h (when the pseudo-steady state of both catalyst is reached at 450 °C). The reaction products have been grouped in: $CO + CO_2$, methane, LPG (C_2–C_4) and C_{5+} hydrocarbons (C_{5+} HC), and their corresponding yields (Eq. (1)) have been determined from the chromatographic analyses. The difference between 100 and the addition of these yields (higher than 70 wt% in all cases) corresponds to the yield of the deposited coke.

Regarding the results obtained with the Pt-Pd/ACP catalyst, an important decrease of the oxygenate yield is observed upon increasing the temperature, what implies an increase of these of $CO + CO_2$, methane, LPG and C_{5+} hydrocarbons. As observed in Fig. 5, rising the temperature from 400 to 450 °C, the increase of methane, LPG and C_{5+} hydrocarbons fractions yields is more pronounced that
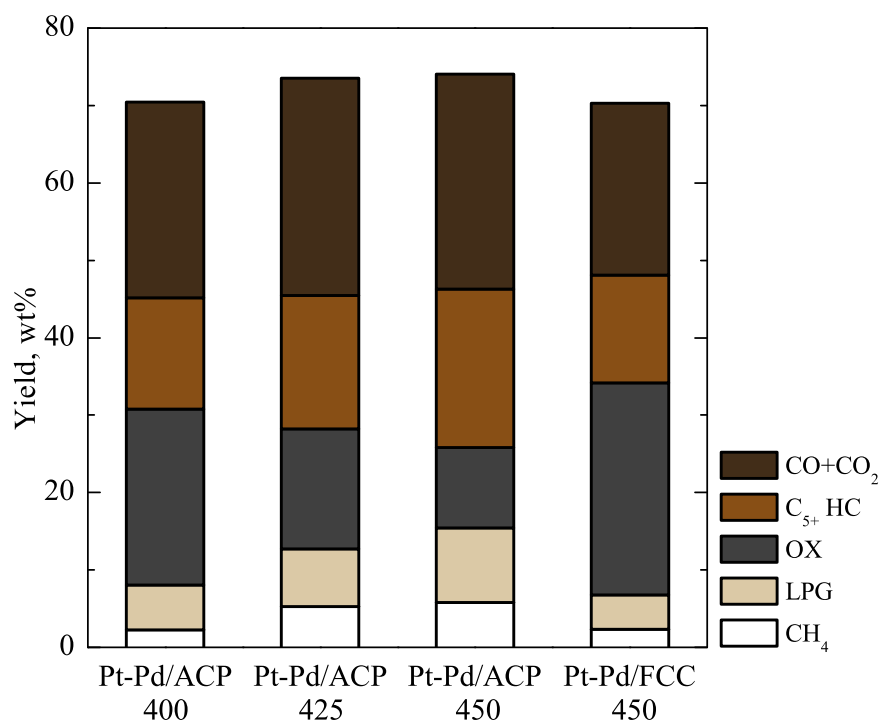
Fig. 5. Product yields obtained for Pt-Pd/ACP catalyst at three temperatures and for Pt-Pd/FCC catalyst at 450 °C.

of $CO + CO_2$, what suggests that the hydrogenation and cracking reactions are selectively favored upon increasing the temperature, in comparison to the decarboxylation and decarbonylation reactions of the oxygenates.

450 °C is the most interesting temperature according to the more stable operation of the process (Fig. 4). Thus, comparing the results of both catalysts at this temperature, it can be observed that Pt-Pd/ACP catalyst has a significantly better performance, with higher yields of C_{5+} hydrocarbons and LPG (20.5 and 9.6 wt%, respectively). On the other side, Pt-Pd/FCC catalyst allows for obtaining lower values of these yields (13.9 and 4.5 wt%, respectively). These results together with the trend of oxygenate yield suggest that the activity of the Pt-Pd/ACP catalyst is significantly higher than that of Pt-Pd/FCC catalyst for the HDO. The gas fraction yield of the catalysts directly correlates with their acidic features, as a higher total acidity leads to higher gas fraction yields.

3.3. Liquid fractions characterization

Fig. 6 shows the composition of the liquid aqueous (Fig. 6a) and organic (Fig. 6b) fractions obtained for the different conditions at TOS = 6 h. Only one liquid phase is observed using the Pt-Pd/ACP catalyst at 400 °C, and in this fraction the main products (referred to the organic liquid fraction) are (Fig. 6a): acetone, 36 wt%; acetic acid, 30 wt%; methanol, 18 wt% and phenols 3.8 wt%. Therefore, this liquid fraction has a high concentration of oxygenates that, together with the high water content (75 wt%), makes the product non-suitable as liquid fuel. Analyzing the liquid fraction obtained at the other temperatures, it is suitable to say that the concentration of methanol, which is the main oxygenated in the aqueous liquid fraction, increases upon increasing the temperature (52 and 58 wt% at 425 and 450 °C, respectively), whereas the acetic acid concentration decreases (24 and 10 wt% at 425 and 450 °C, respectively). On the other hand, the concentration of phenols has the same tendency with the temperature than that of the methanol. This increase of phenol concentration with the temperature is related to the reversible exothermic character of the aromatic hydrogena-

tion, which equilibrium conversion decreases upon increasing the reaction temperature [53].

The aqueous liquid fraction is rich in methanol and acetone, and hence it is interesting as co-feedstock with methanol in the MTO (methanol to olefins) unit in order to obtain olefins, since the phenol concentration is relatively low [54]. The high water content in this fraction does not represent any problem or threat inasmuch as the feeding stream of an industrial MTO process is an equimolecular mixture of methanol and water [55].

The aqueous liquid fraction obtained with the Pt-Pd/FCC catalyst is different than that obtained with Pt-Pd/ACP catalyst. When comparing the performance of Pt-Pd/FCC vs. Pt-Pd/ACP catalysts, the following evidences are observed in Fig. 6a: lower concentrations of methanol (38 vs. 58 wt%) and acetone (12 vs. 23 wt%), and higher concentrations of acetic acid (25 vs. 10 wt%) and phenols (20 vs. 7 wt%). This result confirms the lower activity of the Pt-Pd/FCC to hydrodeoxygenate the phenols of bio-oil, which requires higher activity for hydrodeoxygenation [56].

The organic liquid fraction obtained with the Pt-Pd/ACP catalyst at 425 °C (Fig. 6b) has a high concentration of alkylated aromatics (51 and 21 wt% of 1- and 2+-ring aromatics, respectively) and of naphthenes (19 wt%). The organic liquid fraction also has a 4 wt% of paraffins and iso-paraffins (P + iP) and a 3 wt% of aromatics BTX. Upon the increase of temperature up to 450 °C, a decrease of the concentrations of the 1-ring aromatics (49 wt%) and naphthenes (15 wt%) is observed, whereas these of 2+-ring aromatics (23 wt%) and aromatics BTX (7 wt%) increase. The concentration of paraffins and iso-paraffins remains constant in this range of temperature.

A comparison between the results for Pt-Pd/ACP and Pt-Pd/FCC catalysts at 450 °C, allows for appreciating an increase of the concentration of 1-ring aromatics (49 vs. 51 wt%) and 2+-ring aromatics (23 vs. 35 wt%) and a drop of the ones of paraffins (4 vs. 3 wt%) naphthenes (15 vs. 5 wt%) and aromatics BTX (7 vs. 1 wt%). This result together with that of the trend of water content in the aqueous liquid fraction (Fig. 4) indicates the higher HDO activity of the Pt-Pd/ACP catalyst in the pseudo-steady state. The higher HDO activity of the ACP-based catalyst leads to lower concentrations of acetic
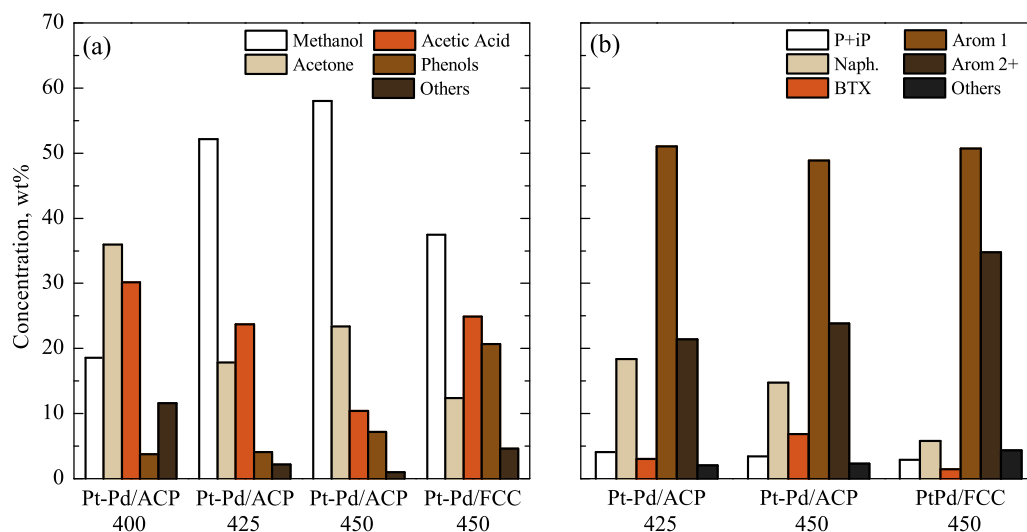
Fig. 6. (a) Aqueous and (b) organic liquid fraction concentrations for Pt-Pd/ACP catalyst at three temperatures and for Pt-Pd/FCC catalyst at 450 °C.

acid and phenols in the aqueous liquid fraction and higher concentrations of naphthenes and BTX in the organic liquid fraction, which enhances the properties of the products as fuel and as raw materials for the petrochemical industry (BTX).

FTIR analyses were performed on the liquid products obtained at 450 °C for the Pt-Pd/ACP catalyst (Fig. 7a) for the ratification of the aforementioned results. According to the literature [57,58], six different vibrational bands were obtained at: (i) 3600–3200 cm^{-1} (O–H stretching), (ii) 3000–2800 cm^{-1} (C–H stretching), (iii) 1750–1650 cm^{-1} (C=O stretching), (iv) 1600–1500 cm^{-1} (aromatic C=C ring breathing), (v) 1450–1350 cm^{-1} (C–H stretching) and (vi) 1300–1000 cm^{-1} (C–O stretching). FTIR spectrum for bio-oil shows the mentioned six vibrational bands, with a high C=O and C–H groups intensity due to its high concentration of acids and esters, and phenols, respectively. FTIR spectra for TOS from 1 to 5 h, until the phase separation is achieved, show that the catalyst deactivates and starts to reach a pseudo-steady state. The O–H band (i) attributed to water, decreases along the time as does the water content of the liquid products; while, the C–H band (ii) increases indicating the formation of hydrocarbons. Once the phase separation occurs, from TOS = 6 h, two different spectra are obtained, one for the aqueous fraction and another one for the organic fraction. In the organic fraction spectra, the six vibrational bands can be observed being majority the C–H (ii), C=C (iv) and the C–H bands (v), attributed to, hydrocarbons, aromatics with various types of substitution and alkanes, respectively. On the other hand, the aqueous fractions, rich in water, methanol and acetic acid, have their highest intensities in the O–H (i) and the C=O bands (iii).

Fig. 7b shows the evolution with the TOS of the relative concentration of alkanes, aliphatics and aromatics in both aqueous and organic liquid fractions calculated from the deconvolution of ^{1}H NMR spectra. Mullen et al. [59] established the regions of each one of the ^{1}H of the groups of interest: alkanes (0.5–1.5 ppm), aliphatics and ^{1}H α-to heteroatom (1.5–3 ppm) and (hetero-) aromatics (4.4–6 ppm). As observed, alkanes and aromatics relative concentrations decrease with TOS in the aqueous liquid fraction whereas aliphatic one increases. Comparing both phases after the phase separation is reached, higher concentrations of alkanes and aromatics and lower of aliphatics are observed in the organic liquid fraction. As methanol and acetic acid appear in the aliphatic region, the drop of aliphatics concentration in the organic liquid fraction is attributed to the removal of oxygenates, which is consistent with the results obtained by FTIR spectroscopy. Likewise, the rise of alkanes and aromatics in the organic liquid fraction correspond to the

appearance of the band (ii) observed in FTIR spectra. These alkane protons are attributed to paraffins, iso-paraffins and naphthenes defined through the chromatographic (GC × GC) measures and the aromatic protons to the BTX, 1- and 2+-ring aromatics also defined. On the other hand, the aromatic protons observed in the aqueous liquid fraction are attributed to phenols, minority components of this phase as shown in Fig. 6a.

Attending to the predominantly aromatic composition of the organic liquid fraction, this fraction requires a further valorization stage of, for example, mild hydrocracking for achieving the suitable hydrocarbon composition to be incorporated into the refinery pools. The HDO treatment of the raw bio-oil studied here should be considered as a preliminary stage of the bio-oil valorization pathway, aiming the removal of oxygenates and water (in the subsequent separation units).

3.4. Gaseous fraction characterization

Regarding the gas fraction, the effect of the temperature on its composition is pronounced, as shown in Fig. 8. The increase of the gas fraction yield (Table 4), along with the higher concentration of methanol in the aqueous liquid fraction, upon increasing the temperature is a result of the cracking reactions favored at higher temperatures. A marked decrease of CO_2 concentration is observed (from 39 to 21 vol%) when the reaction temperature is raised from 400 to 450 °C with the Pt-Pd/ACP catalyst, as well as a small increase of the CO concentration (from 28 to 31 vol%) and a notable one in the methane concentration (from 14 to 26 vol%). In fact, the CO/CO_2 ratio increases from 0.7 to 1.7 (vol/vol) in the temperature range studied (400–450 °C), which is interesting due to the minimization of the CO_2 emissions and the possible enhancement of the gas as a fuel, inasmuch as the fixation of carbon atoms in some of its reduced forms allows for taking advantage of its combustion power.

It is remarkable the absence of olefins in the gas fraction, which are primary products of the cracking reactions. This fact is explained by the activity of the metallic function of the bifunctional catalyst for the hydrogenation of unsaturated bonds of olefins. This function is, nevertheless, unable to hydrogenate unsaturated bonds of aromatics as we explained above.
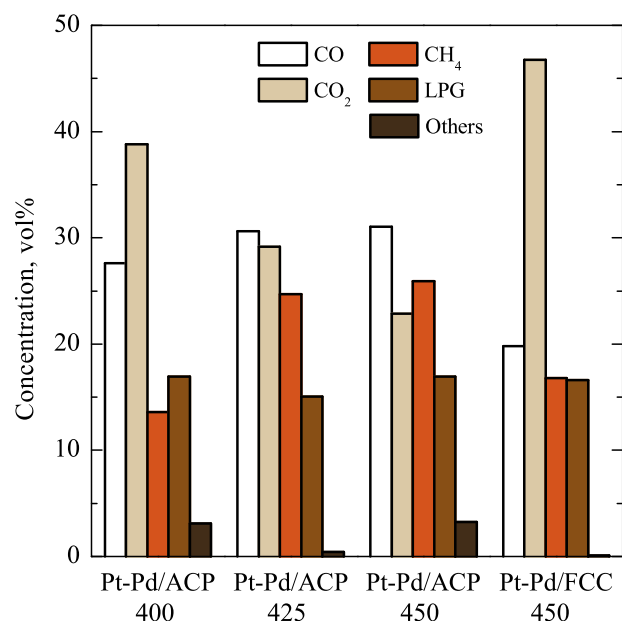
Comparing the composition of the gas fraction at 450 °C for both catalysts, the product obtained with the Pt-Pd/FCC catalyst contains a concentration of CO_2 of 47 vol% (with a CO/CO_2 ratio of 0.4 vol/vol) and lower yields of gas hydrocarbons (Table 4) than that obtained with the Pt-Pd/ACP catalyst, decreasing the interest of this gas frac-

Fig. 8. Gas fraction composition for Pt-Pd/ACP catalyst at three temperatures and for Pt-Pd/FCC catalyst at 450 °C.
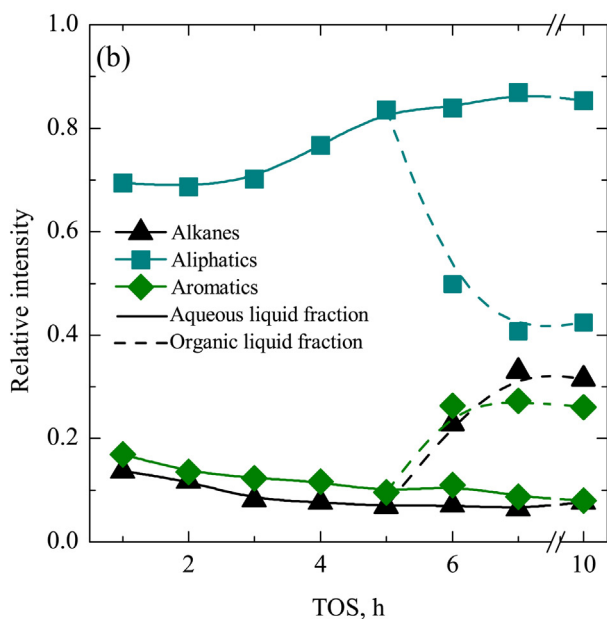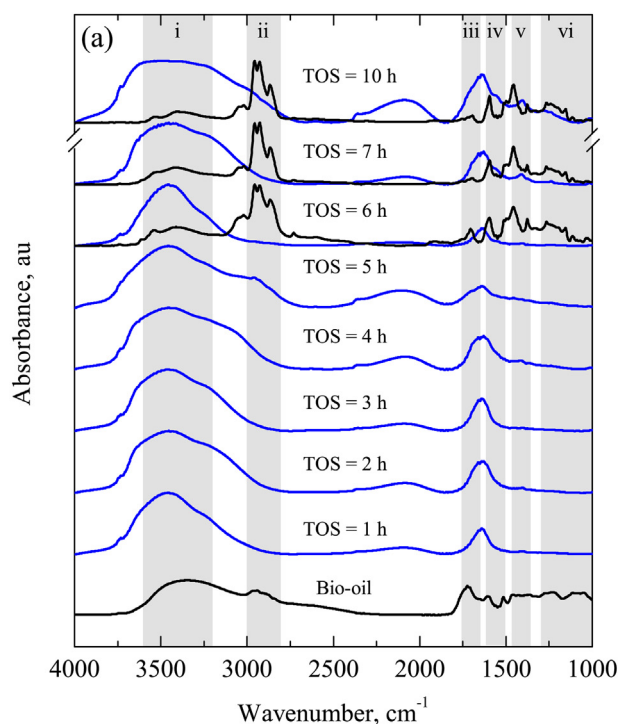
Fig. 7. (a) FTIR spectra of bio-oil and liquid products obtained at 450 °C for the Pt-Pd/ACP catalyst (in blue the aqueous fraction and in black the organic one). (b) Relative evolution of alkane, aliphatic and aromatic relative concentrations with TOS obtained from ^{1}H NMR measures (each fraction has been normalized to one). (For interpretation of the references to colour in this figure legend, the reader is referred to the web version of this article.)

tion as a fuel. These results are consistent with the different acidity of both supports and suggest that at this high temperature, decarboxylation reactions are more favored for the FCC-based catalyst. This undesirable activity for the decarboxylation reactions could be attributed to the presence of other metals like V or Ni held by the support (FCC catalyst). The concentration of this metals according to ICP-OES are: Ni, 846 ppm; and V, 3373 ppm.

3.5. Solid fraction (coke) characterization

The amount of coke deposited (the mass coke content in the final state of the spent catalyst) on the Pt-Pd/ACP catalyst at 400 °C and 6 h on stream is 50.9 wt%, and at 425 °C and 8 h 48.0 wt%. The deposited coke in these two cases, led to the blockage of the reactor. On the other hand, the coke content on the Pt-Pd/ACP catalyst at 450 °C and 10 h is 49.5 wt%, and this value increases up to 62.3 wt% for the Pt-Pd/FCC catalyst at 450 °C and 8 h on stream (reactions without reactor blockage).

This solid fraction (coke) deposited on the catalysts has been characterized by TPO analysis and the DTG curves are shown in Fig. 9. For a correct interpretation of the results, it is worth mentioning that all the weight loss observed for the spent Pt-Pd/FCC catalyst corresponds to coke, whereas for the Pt-Pd/ACP catalyst it corresponds to coke and support, burning the latter at temperatures higher than 520 °C.

Regarding the TPO profiles of the spent Pt-Pd/ACP catalyst, two characteristic combustion peaks (besides the combustion peak of the support) can be observed: (I) the first one at 380 °C, is a well-defined peak attributed to the thermal pyrolytic lignin deposited during the reaction; and (II) the second one at 420 °C, is a shoulder attributed to the carbonaceous structures formed from the oligomers condensation. Coke I is mainly deposited on the external surface of the catalyst and its homogeneous formation, which does not required a catalyst [44], is due to the repolymerization of the phenols of the bio-oil. As a thermal pyrolytic lignin, coke I shows a low-developed structure with high H/C ratio and oxygenated groups [44,46,60]. Coke II is related to a more developed coke (with low H/C ratio) with condensed aromatics species and it is manly deposited on the micro and mesoporous structure of the catalyst as it is formed through condensation reactions on the acidic sites of the catalyst [61,62].

The effect of the reaction temperature on the structure and location of the coke, which is also related to the steady activity state reached by the catalyst at 450 °C, is observed in the notable differences between TPO profiles of Pt-Pd/ACP showed in Fig. 9. As mentioned before, two coke fractions can be identified in the TPO profiles of the spent catalysts, and the amount of each fraction depends on the reaction temperature and on the catalyst activ-
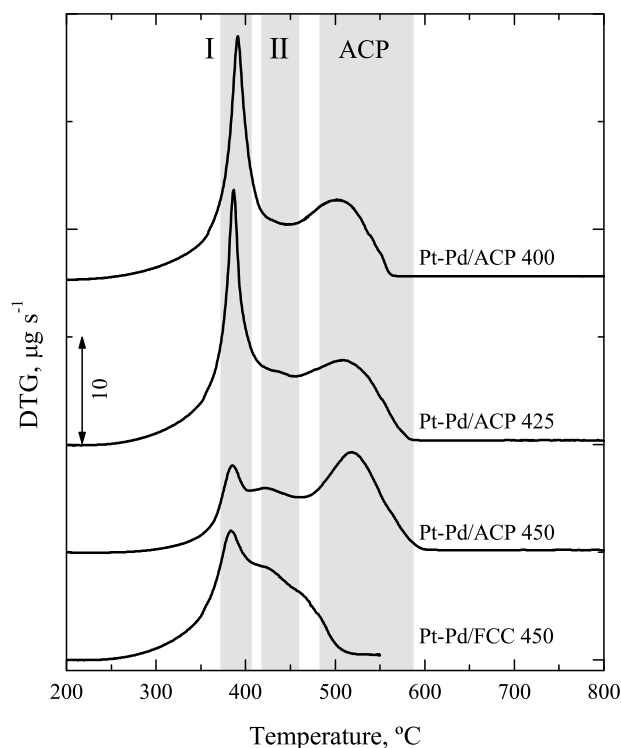
Fig. 9. TPO combustion profiles for Pt-Pd/ACP catalyst at three reaction temperatures and for Pt-Pd/FCC at 450 °C.

ity. TPO profiles of the spent catalysts at 400 and 425 °C exhibit an intense peak attributed to coke I and a less visible shoulder corresponding to coke II. The smaller peak of the coke I corresponds to the higher reaction temperature (450 °C) and to the higher activity of the catalyst. These two factors favor the transformation of the bio-oil phenols, and mitigates the repolymerization reactions that lead to the formation of the thermal pyrolytic lignin. However, they benefit the hydrocarbons production, which are the precursors of the coke II observed in the TPO profile of the spent catalyst at the highest reaction temperature.

On the other hand, the TPO profile of the coke deposited on the Pt-Pd/FCC catalyst at 450 °C corresponds to a more heterogeneous coke in composition and location. The shape of the peak attributed to coke I is similar to that of spent Pt-Pd/ACP at the same reaction temperature, suggesting that the deposition of the thermal pyrolytic lignin is controlled at this temperature, and it leads to the catalyst pseudo-steady state. However, in this case, the intensity of the shoulder attributed to coke II is slightly reduced. This fact could be related to the *meso-* and macroporous structure of the FCC support, which eases the deposition of the thermal pyrolytic lignin inside the porous matrix, yielding a more heterogeneous coke. This solid fraction burns at higher temperature, from bigger to smaller pore sizes due to the oxygen diffusion facility, reaching the complete combustion of the deposited coke at ca. 500 °C [47].

Comparing the TPO results of both spent catalysts at 450 °C with their remaining activity after reaching the pseudo-steady state (Fig. 4), it is possible to conclude that the porous structure of the ACP support is more appropriated than that of the FCC support to preserve the metallic and acidic sites because of the microporous character of ACP allows for retaining the thermal pyrolytic lignin (coke I) on the external surface of the catalyst, whereas the FCC matrix favors its deposition within the pores on the active sites.

The high stability of Pt-Pd/ACP catalyst at 450 °C, up to 10 h without reactor blockage, is an interesting starting point for industrial scale up of the process. However, taking the previous industrial experience in hydrotreating and hydrocracking residues, a rational approach would be using expanded or ebullated bed reactor (with moving catalytic particles allowing the continuous withdrawal of the catalyst, with industrial implementations like the LC-fining process) to cope with the severe coke deposition [63].

4. Conclusions

Pt-Pd/ACP catalyst shows an outstanding performance (activity and hydrocarbons selectivity) but particularly stability in the HDO of raw bio-oil, reaching a steady activity at 450 °C after 6 h on stream. This effect is due to the simultaneous formation and hydrocracking of the coke deposited on the catalyst, which causes the active sites blockage. This is an encouraging result for using stable acid activated carbon supports in the HDO of bio-oil, intensifying the valorization of products obtained from lignocellulosic biomass.

HDO results are very favorable, in spite of the high water content observed in the reaction media. A notable hydrocarbons liquid yield (20 wt%) is obtained at 450 °C, as well as a gas fraction useful as a fuel with high concentration (77 wt%) of methane, LPG and CO. The amount of aromatics in the organic liquid fraction (BTX, 1- and 2+-ring aromatics, 80 wt%) excludes its direct applications as fuel. Therefore, these results are interesting for a first stage of raw bio-oil valorization, with the aim of obtaining a hydrocarbon fraction which could be co-fed to a mild hydrocracking unit in order to produce lighter hydrocarbons, which could be incorporated to the refinery pools.

It is remarkable the high methanol concentration in the aqueous liquid fraction, which composition is especially interesting because it can be valorized by co-feeding it (with pure methanol) into the MTO process. This byproduct stream does not require any pretreatment since the water content is not an issue in the MTO process.

The high stability of Pt-Pd/ACP catalyst in this kind of hydroprocessing conditions is an interesting feature in order to operate for longer reaction runs, what should require an appropriate reactor, like a moving bed reactor with catalyst circulation allowing the separation of the thermal pyrolytic lignin deposited in the external surface of the catalyst.

Acknowledgements

References

[1] D. Meier, B. Van De Beld, A.V. Bridgwater, D.C. Elliott, A. Oasmaa, F. Preto, Renew. Sust. Energy Rev. 20 (2013) 619–641.
[2] A. Sanna, Bioenergy Res. 7 (2014) 36–47.
[3] M. Patel, X. Zhang, A. Kumar, Renew. Sust. Energy Rev. 53 (2016) 1486–1489.
[4] D. Carpenter, T.L. Westover, S. Czernik, W. Jablonski, Green Chem. 16 (2014) 384–406.
[5] Z. Yang, A. Kumar, R.L. Huhnke, Renew. Sust. Energy Rev. 50 (2015) 859–870.
[6] A.R.K. Gollakota, M. Reddy, M.D. Subramanyam, N. Kishore, Renew. Sust. Energy Rev. 58 (2016) 1543–1568.
[7] A. Atutxa, R. Aguado, A.G. Gayubo, M. Olazar, J. Bilbao, Energy Fuels 19 (2005) 765–774.
[8] A. Aho, N. Kumar, K. Eränen, T. Salmi, M. Hupa, D.Y. Murzin, Fuel 87 (2008) 2493–2501.
[9] E.F. Iliopoulou, S.D. Stefanidis, K.G. Kalogiannis, A. Delimitis, A.A. Lappas, K.S. Triantafyllidis, Appl. Catal. B: Environ. 127 (2012) 281–290.
[10] K. Iisa, R.J. French, K.A. Orton, M.M. Yung, D.K. Johnson, J. ten Dam, M.J. Watson, M.R. Nimlos, Energy Fuels 30 (2016) 2144–2157.
[11] Q. Bu, H. Lei, A.H. Zacher, L. Wang, S. Ren, J. Liang, Y. Wei, Y. Liu, J. Tang, Q. Zhang, R. Ruan, Bioresour. Technol. 124 (2012) 470–477.

[12] M. Saidi, F. Samimi, D. Karimipourfard, T. Nimmanwudipong, B.C. Gates, M.R. Rahimpour, Energy Environ. Sci. 7 (2014) 103–129.
[13] P.M. Mortensen, J.D. Grunwaldt, P.A. Jensen, K.G. Knudsen, A.D. Jensen, Appl. Catal. A Gen. 407 (2011) 1–19.
[14] M. Al-Sabawi, J. Chen, S. Ng, Energy Fuels 26 (2012) 5355–5372.
[15] E. Furimsky, Catal. Today 217 (2013) 13–56.
[16] A. Corma, G.W. Huber, L. Sauvanaud, P. O'Connor, J. Catal. 247 (2007) 307–327.
[17] M. Bertero, U. Sedran, Catal. Today 212 (2013) 10–15.
[18] M. Bertero, G.D. La Puente, U. Sedran, Renew. Energy 60 (2013) 349–354.
[19] N. Thegarid, G. Fogassy, Y. Schuurman, C. Mirodatos, S. Stefanidis, E.F. Iliopoulou, K. Kalogiannis, A.A. Lappas, Appl. Catal. B: Environ. 145 (2014) 161–166.
[20] A. Ibarra, E. Rodriguez, U. Sedran, J.M. Arandes, J. Bilbao, Ind. Eng. Chem. Res. 55 (2016) 1872–1880.
[21] G.W. Huber, J.N. Chheda, C.J. Barret, J.A. Dumesic, Science 308 (2005) 1446–1450.
[22] T.P. Vispute, G.W. Huber, Green Chem. 11 (2009) 1433–1445.
[23] D.C. Elliott, Energy Fuels 21 (2007) 1792–1815.
[24] D.C. Elliott, T.R. Hart, Energy Fuels 23 (2009) 631–637.
[25] A. Zacher, M. Olarte, D. Santosa, Green Chem. 16 (2014) 491–515.
[26] Z.B. Wang, C.Z. Li, D.M. Gu, G.P. Yin, J. Power Sources 238 (2013) 283–289.
[27] D.E. Resasco, J. Phys. Chem. Lett. 2 (2011) 2294–2295.
[28] X. Zhu, L. Nie, L.L. Lobban, R.G. Mallinson, D.E. Resasco, Energy Fuels 28 (2014) 4104–4111.
[29] E. Lam, J.H.T. Luong, ACS Catal. 4 (2014) 3393–3410.
[30] D.C. Elliott, T.R. Hart, G.G. Neuenschwander, L.J. Rotness, M.V. Olarte, A.H. Zacher, Y. Solantausta, Energy Fuels 26 (2012) 3891–3896.
[31] A. Sanna, T.P. Vispute, G.W. Huber, Appl. Catal. B: Environ. 165 (2015) 446–456.
[32] I. Hita, T. Cordero-Lanzac, A. Gallardo, J.M. Arandes, J. Rodríguez-Mirasol, J. Bilbao, T. Cordero, P. Castaño, Catal. Commun. 78 (2016) 45–51.
[33] J. Bedia, R. Ruiz-Rosas, J. Rodríguez-Mirasol, T. Cordero, AIChE J. 56 (2010) 1557–1568.
[34] J. Bedia, J.M. Rosas, J. Márquez, J. Rodríguez-Mirasol, T. Cordero, Carbon 47 (2009) 286–294.
[35] J. Bedia, R. Barrionuevo, J. Rodríguez-Mirasol, T. Cordero, Appl. Catal. B: Environ. 103 (2011) 302–310.
[36] P. Castaño, D. van Herk, M.T. Kreutzer, J.A. Moulijn, M. Makkee, Appl. Catal. B: Environ. 88 (2009) 213–223.
[37] I. Hita, E. Rodríguez, M. Olazar, J. Bilbao, J.M. Arandes, P. Castaño, Energy Fuels 29 (2015) 5458–5466.
[38] J. Bedia, R. Ruiz-Rosas, J. Rodríguez-Mirasol, T. Cordero, J. Catal. 271 (2010) 33–42.
[39] A.R. Fernandez-Akarregi, J. Makibar, G. Lopez, M. Amutio, M. Olazar, Fuel Process. Technol. 112 (2013) 48–56.
[40] I. Hita, R. Palos, J.M. Arandes, J.M. Hill, P. Castaño, Fuel Process. Technol. 144 (2016) 239–247.
[41] D. van Herk, P. Castaño, M. Quaglia, M.T. Kreutzer, M. Makkee, J.A. Moulijn, Appl. Catal. A: Gen. 365 (2009) 110–121.
[42] G. Elordi, M. Olazar, P. Castaño, M. Artetxe, J. Bilbao, Ind. Eng. Chem. Res. 51 (2012) 14008–14017.
[43] J.M. Rosas, R. Ruiz-Rosas, J. Rodríguez-Mirasol, T. Cordero, Carbon 50 (2012) 1523–1537.
[44] A. Ochoa, B. Aramburu, M. Ibáñez, B. Valle, J. Bilbao, A.G. Gayubo, P. Castaño, ChemSusChem 7 (2014) 2597–2608.
[45] A.G. Gayubo, B. Valle, A.T. Aguayo, M. Olazar, J. Bilbao, J. Chem. Technol. Biotechnol. 85 (2010) 132–144.
[46] B. Valle, P. Castaño, M. Olazar, J. Bilbao, A.G. Gayubo, J. Catal. 285 (2012) 304–314.
[47] P. Castaño, A. Gutiérrez, I. Hita, J.M. Arandes, A.T. Aguayo, J. Bilbao, Energy Fuels 26 (2012) 1509–1519.
[48] A. Oasmaa, E. Kuoppala, A. Ardiyanti, R.H. Venderbosch, H.J. Heeres, Energy Fuels 24 (2010) 5264–5272.
[49] R.H. Venderbosch, A.R. Ardiyanti, J. Wildschut, A. Oasmaa, H.J. Heeres, J. Chem. Technol. Biotechnol. 85 (2010) 674–686.
[50] J. Wildschut, M. Iqbal, F.H. Mahfud, I.M. Cabrera, R.H. Venderbosch, H.J. Heeres, Energy Environ. Sci. 3 (2010) 962–970.
[51] G.S. Foo, A.K. Rogers, M.M. Yung, C. Sievers, ACS Catal. (2016) 1292–1307.
[52] A. Gutiérrez, J.M. Arandes, P. Castaño, A.T. Aguayo, J. Bilbao, Energy Fuels 25 (2011) 3389–3399.
[53] I. Hita, A.T. Aguayo, M. Olazar, M.J. Azkoiti, J. Bilbao, J.M. Arandes, P. Castaño, Energy Fuels 29 (2015) 7542–7553.
[54] A.G. Gayubo, A.T. Aguayo, A. Atutxa, R. Aguado, M. Olazar, J. Bilbao, Ind. Eng. Chem. Res. 43 (2004) 2619–2626.
[55] P. Tian, Y. Wei, M. Ye, Z. Liu, ACS Catal. 5 (2015) 1922–1938.
[56] C.V. Loricera, P. Castaño, A. Infantes-Molina, I. Hita, A. Gutiérrez, J.M. Arandes, J.L.G. Fierro, B. Pawelec, Green Chem. 14 (2012) 2759–2770.
[57] C. Lievens, D. Mourant, M. He, R. Gunawan, X. Li, C.Z. Li, Fuel 90 (2011) 3417–3423.
[58] Y. Luo, V.K. Guda, E.B. Hassan, P.H. Steele, B. Mitchell, F. Yu, Energy Convers. Manag. 112 (2016) 319–327.
[59] C.A. Mullen, G.D. Strahan, A.A. Boateng, Energy Fuels 23 (2009) 2707–2718.
[60] M. Ibáñez, B. Valle, J. Bilbao, A.G. Gayubo, P. Castaño, Catal. Today 195 (2012) 106–113.
[61] C.H. Bartholomew, Appl. Catal. A: Gen. 212 (2001) 17–60.
[62] M. Guisnet, P. Magnoux, Appl. Catal. A: Gen. 212 (2001) 83–96.
[63] K.M. Sundaram, U. Mukherjee, M. Baldassari, Energy Fuel 22 (2008) 3226–3236.